Fabrication and structural analysis of Al, Ga, and In nanocluster crystals

Jin-Feng Jia,[1] Xi Liu,[1] Jun-Zhong Wang,[1] Jian-Long Li,[1] X. S. Wang,[1] Qi-Kun Xue,[1] Zhi-Qiang Li,[2] Zhenyu Zhang,[3] and S. B. Zhang[4]

[1]*State Key Laboratory for Surface Physics, Institute of Physics, Chinese Academy of Sciences, Beijing 100080, China*
[2]*Steacie Institute for Molecular Sciences, National Research Council of Canada, Ottawa, Ontario, K1A 0R6, Canada*
[3]*Oak Ridge National Laboratory, Oak Ridge, Tennessee 37831-6032*
[4]*National Renewable Energy Laboratory, Golden, Colorado 80401*

(Received 19 May 2002; published 23 October 2002)

Artificial nanocluster crystals of In, Ga, and Al were fabricated using a technique in which surface mediated magic clustering is used to achieve identical cluster size while the Si(111)-7×7 surface is used as a template for ordering the clusters. The atomic structures, formation mechanism and stability of the nanoclusters were studied with *in situ* scanning tunneling microscopy combined with first-principles total energy calculations. Our study shows that delicate control of growth kinetics is extremely important for cluster crystal fabrication, and there is essentially no limitation to this method. The high thermal stability and unique structure make these artificial nanocluster crystals promising for various applications.

DOI: 10.1103/PhysRevB.66.165412 PACS number(s): 81.07.−b, 68.37.Ef, 68.43.Bc, 61.46.+w

I. INTRODUCTION

In the last decade, fabrication and understanding of nanoclusters have become exciting areas of research.[1–11] This is driven by their great potential in technology applications and scientific importance in bridging our understanding between molecular and condensed matter physics. The beneficial structural, electronic, optical, magnetic, and chemical properties of nanoclusters can be employed in many fields, such as nanocatalysis,[1,2] optical and electronic devices,[3,4] single-electronic devices,[5] ultrahigh-density magnetic recording,[6–8] quantum computing, and quantum cryptography.[9] The properties of nanoclusters are size and composition specific, so it is possible to design materials with desired properties by choosing the correct size and composition of clusters. Their special properties may, however, be degraded by the inhomogeneity in nanocluster materials with broad size distribution and random spatial arrangements. It therefore becomes critical for their practical application to fabricate stable, ordered, and identical-sized nanocluster arrays. Further more, from the viewpoint of fundamental research, a periodic array of identical nanoclusters is an ideal model system for the study of single nanoclusters and interactions between them. In many aspects, nanoclusters are artificial atoms,[9,12] so, a periodic lattice made up of the clusters with the same nanometer size is an artificial crystal. This form of condensed matter provides unprecedented opportunities for exploring the laws of physics.

Tremendous efforts have been made to achieve size uniformity and spatial control in fabrication of nanoclusters using various methods, such as self-organization in heterogeneous strained thin-film growth[13,14] lithography methods,[15,16] focused ion beam,[5] scanning probe microscope,[17,18] and self-assembly in chemical synthesis.[6,11] Although nanocluster/dot aggregates with fairly good size uniformity and spatial distribution have been fabricated,[14,19–21] it is still very difficult to fabricate perfectly ordered identical-sized nanocluster arrays, the so-called artificial nanocluster crystals.

Recently, we explored a technique of "template and surface-mediated magic clustering" and demonstrated that fabrication of artificial cluster crystals is possible.[22,23] In this paper, we report the details of the fabrication of artificial nanocluster crystals of Al, Ga, and In and present a systematic study on their atomic structures by using *in situ* scanning tunneling microscopy (STM) combined with first-principles total energy calculations. By comparing different formation conditions, we can draw the conclusion that delicate control of the growth kinetics is crucial for their fabrication. The different stabilities and electronic states are also discussed based on their atomic structure as established from STM analysis and theoretical calculations.

II. EXPERIMENT

The experiments were carried out with an OMICRON variable temperature STM operated in ultrahigh vacuum (base pressure $\sim 5\times10^{-11}$ Torr).[22–24] The system has two chambers containing STM, LEED, Auger electron spectroscopy (AES), and MBE facilities. The samples were introduced into the vacuum chamber via a load lock and prepared in the MBE chamber. A magnetically coupled feed through is used for sample transfer between the MBE chamber and the analysis chamber where the LEED/AES as well as STM inspection can be performed. The STM can be operated at a temperature range from 25 to 1000 K. The samples were heated by electric current directly through them, and the sample temperatures were monitored by an infrared pyrometer. A chemically etched tungsten tip was used as the STM probe.

The Si(111) samples (As doped, 0.1 Ohm cm) were degassed at about 500 °C for several hours after being introduced into the vacuum chamber without any chemical treatment. Preparation of the clean surface was performed by flashing to ~1200 °C while keeping the vacuum better than 1×10^{-9} mbar. The cleanliness and ordering of the samples were checked by LEED, AES, and STM. Well-ordered Si(111)7×7 surfaces can normally be obtained after cleaning. Three boron nitride crucibles were used to produce Al,

 ©2002 The American Physical Society

Ga, and In (purity 99.9999%) atomic beams. All STM images reported here were recorded at constant current mode with a tunneling current of 20 to 100 pA.

III. RESULTS AND DISCUSSIONS

A. Method to fabricate the artificial nanocluster crystals

To fabricate the artificial nanocluster crystals, we have to solve two problems. The first is to make all nanoclusters identical and the second is to arrange them in perfect order. Since thermodynamic fluctuations and other growth uncertainties always exist during growth, it is impossible to grow identical nanoclusters or arrange them in order with usual self-organization growth methods.

In this study, in order to make all clusters identical, our strategy is to employ some stable identical-sized entity as a building block for assembling the nanocluster array. Surface-mediated magic clusters are a good candidate as such an entity.[22,23] As discovered in the 1980's for the gas phase,[25] certain clusters with specific numbers of atoms (magic clusters) exhibit a closed electronic and/or atomic shell structure and remarkable stability. Recently, several studies demonstrate that surface-mediated clusters of specific or "magic" sizes indeed exist with remarkable stability.[26–29] As the surface interacts with the clusters, the interaction may modify the magic sizes and influence their stability. On the other hand, such an interaction could also provide a way to arrange the clusters in order automatically by selecting a proper periodic template and optimizing growth kinetics so that a trade-off between the two processes could be realized. Thus, in order to order the clusters, the second key point is the periodic template substrate for site-specific nucleation of the clusters if they could indeed form on such substrate. It turns out that Si(111)7×7 is an ideal template. The Si(111)-7×7 surface[30] is one of the most technically important semiconductor surfaces. It is very stable and its atomic structure has been extensively investigated and is now well established. As shown in Fig. 1, one unit cell of Si(111)-7×7 contains 12 Si adatoms and 6 rest atoms, which are divided into two different half unit cells by Si dimers. There is a stacking fault between the second and third layer atoms in the left half unit cell (the interlayer bonding rotates 60°), the faulted half unit cell (FHUC), which makes the FHUC more reactive than the unfaulted half (UFHUC), (the right half of the figure). The unit cell size (2.7 nm×2.7 nm) is comparable to the Fermi wavelength of electrons in most metals. Therefore, it is conceivable to fabricate ordered arrays of identical quantum dots if magic clusters can be grown on this surface without breaking the surface periodicity.[31] In this context, as long as atoms of the selected metal can form clusters of definite size on such a template, there is no limitation to this strategy.

In order to form uniform nanocluster arrays by taking advantage of magic clustering on a Si(111)7×7 template, growth parameters must be designed very carefully. If the substrate temperature during deposition is too low (room temperature or lower) and the deposition flux is too high, the mobility of the atoms is too low to move and aggregate into magic clusters, or they are too slow to arrive at the predesigned destination before meeting other atoms to form immobile nuclei and smaller clusters.[32] On the other hand, "hot landing" at high temperature may make the atoms too energetic. They may either form a strong bond to a Si atom (reconstruction occurs) or coalesce to large islands. (At higher temperature, say, 400 °C, even the large islands collapse and phase transition into the $\sqrt{3}\times\sqrt{3}$ takes place.) Low deposition flux will lead to too few nuclei and large clusters by Ostwald ripening. Since the number of atoms in a magic cluster takes a *discrete value*, periodic arrays for given-size magic clusters can be achieved by a delicate balance of the growth parameters—the kinetics have to be manipulated in such a way that the atom hopping rate between the two halves of the Si(111)-7×7 unit cell can exceed the arrival rate of atoms (in order to complete ordering), and the island ripening must remain below the regime for forming the next larger magic number cluster. The importance of kinetic parameters will be further discussed later.

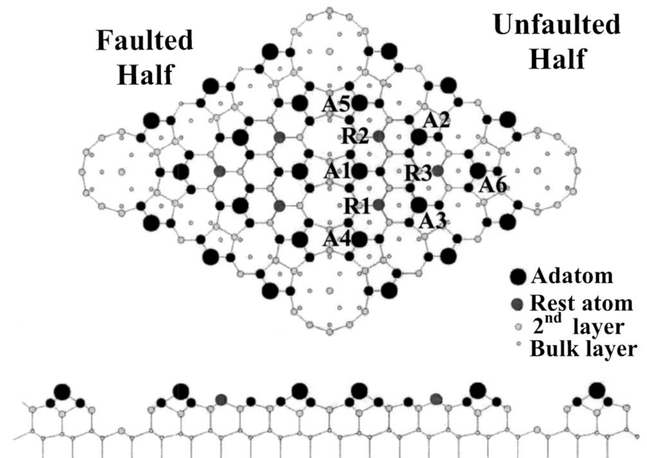

FIG. 1. (a) Top view and (b) side view of the dimer-adatom-stacking fault (DAS) model of the Si(111)-7×7 surface proposed by Takayanagi *et al.* (Ref. 29). There is a stacking fault between the second and third layers atoms at the right half unit cell, the faulted half unit cell (FHUC), which makes the FHUC more reactive than the unfaulted HUC (UFHUC, the left half) in the diamond structure of Si. The sites relevant to the discussion are indicated as $R1-R3$ for Si rest atoms and $A1-A6$ for Si adatoms.

B. Fabrication of In, Ga, and Al artificial nanocluster crystals

If the substrate is held at high temperature (above 400 °C) during In deposition, In-induced surface reconstruction will result, which bas been extensively investigated previously.[33] If the substrate is held at room temperature or lower, a featureless surface will appear.[32] Identical clusters can only be obtained when the Si(111)-7×7 substrate is held at 100–220 °C.[21] As shown in Fig. 2(a), after deposition of about 0.05 ML of In, all the In adatoms form identical nanoclusters: each cluster is imaged as a hollow-centered equilateral triangle consisting of six white spots. It can also be noticed that most of the clusters occupy the FHUC of Si(111)-7×7, and even at low coverage local ordering is already evident. Our statistical analysis (by sampling more

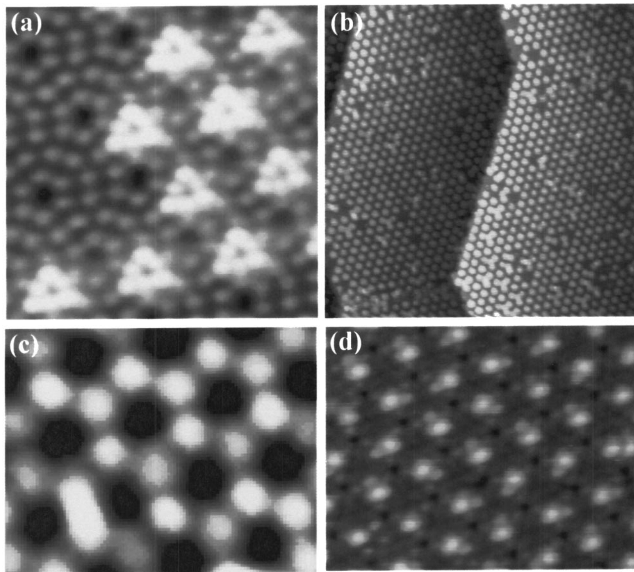

FIG. 2. Scanning tunneling microscope (STM) images of In nanostructures on Si(111). (a) In nanocluster at ~0.05 ML coverage (1 ML=one adsorbed atom per substrate atom. The image size ~8 nm×8 nm, deposition rate ~0.05 ML/min and temperature ~120 °C). (b) Perfectly ordered In nanocluster arrays at ~0.12 ML In coverage (the image size ~80 nm×80 nm). The image shows high uniformity in terms of cluster size. (c) Perfectly ordered honeycomb structure of In nanocluster arrays at ~0.2 ML In coverage (the image size ~8 nm×6 nm). (d) In nanocluster formed at incorrect conditions (the image size ~15 nm×12 nm).

than 3000 clusters at this coverage) shows that about 92% of the clusters occupy the FHUC and 8% the UFHUC. The adsorption energy difference between the two halves of the 7×7 unit cell can be estimated by applying the Boltzmann distribution $N_F/N_U=\exp(-\Delta E/kT)$ (Ref. 20), where N_F and N_U are the occupation numbers on the FHUC and UFHUC at temperature T, respectively. ΔE is the energy difference, and k is the Boltzmann constant. According to our statistical results from the STM images, $\Delta E=0.08\pm0.01$ eV.

Increasing the In coverage to 0.12 ML, a perfectly ordered nanocluster array forms as shown in Fig. 2(b). In the image, each bright spot corresponds to an In cluster. Except for some inhomogeneities caused by defects or locally overdeposited In, the ordering of the clusters is essentially perfect. Considering each cluster as an artificial atom, this periodic lattice of identical clusters represents a new artificial crystal. With every cluster occupying the FHUC and a nearest neighbor distance of 2.7 nm, the geometry of this "lattice" is the same as that of the Si(111)-7×7.

Further increasing the In coverage, In clusters will occupy the UFHUC's of Si(111)-7×7. These clusters in UFHUC's exhibit basically the same appearance as those in the FHUC's [Fig. 2(a)]. At a coverage of ~0.24 ML, a characteristic ordered honeycomb structure develops [as shown in Fig. 2(c)] due to equivalent occupation of both halves of the unit cell. In the STM image, In clusters in FHUC's appear a little bit brighter than those in UFHUC's.

If the deposition conditions fall out the right range, different clusters could result, as shown in Fig. 2(d). In this case, the clusters still take the position of FHUC and form an ordered array. However, the appearances of all clusters are different from the hollow-centered equilateral triangle consisting of 6 white spots observed for normal In clusters. In the empty state STM image, only one very bright spot was imaged at a corner of the triangle. Their structure will be further discussed later.

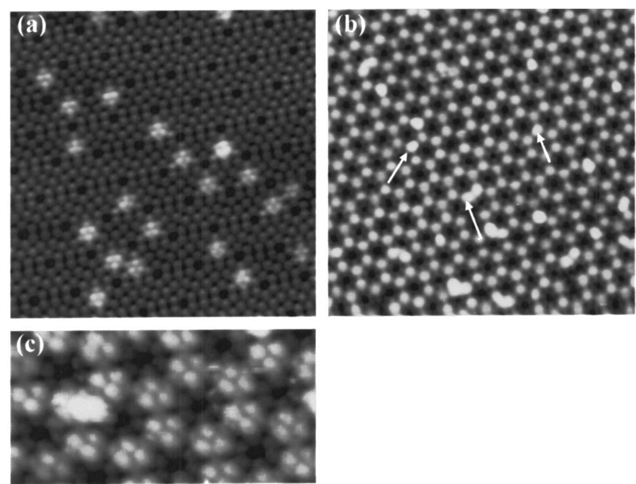

FIG. 3. STM images of Ga nanostructures on Si(111). (a) Ga nanocluster at ~0.05 ML, 20 nm×20 nm. (b) Perfectly ordered honeycomb structure of Ga nanocluster arrays at ~0.24 ML coverage, 32 nm×32 nm (deposition rate ~0.02 ML/min and temperature ~180 °C). (c) High resolution STM image of the structure in (b′), 10 nm×7 nm.

Ga nanoclusters are relatively easy to fabricate. Room-temperature deposition already results in nanoclusters even at very low coverage.[34] Ga nanoclusters formed at a coverage of 0.05 ML are shown in Fig. 3(a). In the empty state STM image, Ga clusters also appear triangular and reside at the center of either half of the Si(111)7×7 unit cell. Each cluster contains six bright spots, the three on the edge are brighter than those at the corner, which is quite different from the In clusters, where the three spots on the edges of the triangle appear darker than the three at the corner. In the case of Ga, the clusters occupy both halves of the unit cell of Si(111)-7×7 even at low coverage.[34] Our statistical analysis shows that the clusters occupy the FHUC and UFHUC almost equally, which is totally different from the behavior of the In clusters. According to the Boltzmann distribution, the adsorption energy difference between the two halves of the 7×7 unit cell is negligible within the error.

With increasing Ga coverage, the numbers of clusters in both halves of the 7×7 unit cell increase equally. Heating the sample to a temperature of 150–250 °C during deposition could result in a more uniform nanocluster array. At a coverage of approximately 0.24 ML, an ordered honeycomb structure forms as shown in Fig. 3(b). In artificial Ga nanocluster crystals, each unit cell contains two Ga clusters. The Ga clusters in FHUC are brighter than those in UFHUC when imaged at a positive bias. There are some abnormal bright spots, as indicated by the arrows in Fig. 3(b). Most of them have the same appearance as the normal Ga clusters in

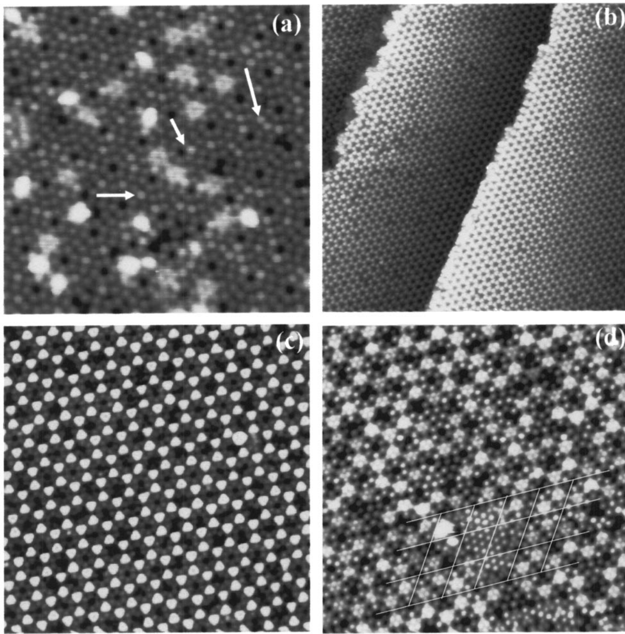

FIG. 4. (a) Empty state STM image (20 nm×20 nm) of the Si(111)-7×7 adsorbed with 0.05 ML Al. The white arrows indicate the Al atoms adsorbed on the top of Si adatoms. Sample bias voltage $V_s = 2.0$ V. (b) Perfectly ordered Al nanocluster array at ~0.25 ML Al coverage. The image was obtained at $V_s = 2.0$ V, the image size is 100 nm×100 nm (deposition rate ~0.01 ML/min and temperature ~300 °C). (c) Close view of the Al nanocluster array in (b). $V_s = -2.0$ V, the image size is 30 nm×30 nm. (d) Coexistence of Si(111) $\sqrt{3}\times\sqrt{3}$-Al, $\sqrt{7}\times\sqrt{7}$-Al, and Al nanoclusters after annealing the sample in (b) at about 550 °C. The image size is 25 nm×25 nm and $V_s = 1.2$ V.

the atomic resolution STM images, therefore, this contrast change has an electronic origin. However, some of the big bright spots could be caused by excess Ga or other impurities since no atomic resolution images could be obtained for them, as shown in Fig. 3(c). In the very high resolution STM image shown in Fig. 3(c), we can see that the most noticeable features are the three spots on the edge of the triangle, while the three at the corner are almost invisible.

If Al is deposited at room temperature, we can see many individual Al atoms adsorbed on the top of the Si adatoms as indicated by the white arrows in Fig. 4(a). Some Al clusters are also observed (the big bright spots in the image).[23] With increasing Al coverage, more clusters are formed, but the sizes of the clusters are not uniform. At 0.2 ML coverage, a featureless structure consisting of irregular clusters develops, which smears out the 7×7 symmetry of the Si substrate. For the deposition rate given above, an ordered identical Al clusters array can be formed only when the substrate temperature is higher than 200 °C. A large scale STM image of the Al nanoclusters is shown in Fig. 4(b), and we can clearly see that the cluster array is very uniform in this large area. Larger area scans and scans at different locations reveal that the cluster array is even uniform over the whole sample surface (~2×9 mm^2). A zoom-in STM image (at negative sample bias) is shown in Fig. 4(c), which further demonstrates that all Al clusters are identical and that their arrangement is perfectly periodic. Similar to the Ga clusters, the Al clusters equally occupy both halves of the Si(111)-7×7 unit cell forming a characteristic honeycomb structure. Considering each cluster as an artificial atom, this periodic lattice of the same-sized clusters represents a new artificial crystal. Among the nanoclusters made by this method, the uniformity and ordering of the Al clusters are the best.

In addition, the Al nanocluster array is stable and can survive even at an annealing temperature up to 500 °C. After annealing the Al nanocluster array [shown in Figs. 4(b) and 4(c)] at about 550 °C, small areas with the $\sqrt{3}\times\sqrt{3}$-Al and $\sqrt{7}\times\sqrt{7}$-Al appear and coexist with the Al nanoclusters, as shown in Fig. 4(d). According to the atomic structure models of the Si(111)$\sqrt{3}\times\sqrt{3}$-Al and $\sqrt{7}\times\sqrt{7}$-Al, each $\sqrt{3}\times\sqrt{3}$ unit cell contains one Al atom while the $\sqrt{7}\times\sqrt{7}$ unit cell three Al atoms.[35] Assuming that all Al atoms forming the $\sqrt{3}\times\sqrt{3}$-Al or $\sqrt{7}\times\sqrt{7}$-Al reconstruction come from the clusters in the same area (this is true as no noticeable change in the surrounding areas could be observed), the number of the total Al atoms in the reconstruction area can be easily calculated. With this simple method, each Al cluster is determined to contain 6 ± 1 Al atoms (such calibration was done also for the Ga and ln clusters, and a similar result was obtained).

In the high resolution STM image [Fig. 4(d)], the Al clusters appear triangular and reside at the center of each half of the Si(111)-7×7 unit cell. Each cluster contains six bright spots, the three on the edge are brighter than those at the corner. The empty state STM image of the Al cluster is very similar to that of the Ga cluster shown in Fig. 3 as well as observed by Lai and Wang.[34] However, it is different from that of the In cluster shown in Fig. 2, where the three spots on the edges of the triangle appear darker (also see Ref. 23).

C. Structure of In, Ga, and Al artificial nanocluster crystals

To better understand the basic principles governing the array formation process, we have studied systematically the atomic structures of the In, Ga, and Al clusters. The atomic resolution STM images of the In clusters at different sample biases (+0.6 V, +0.2 V, and −0.3 V, respectively) are shown in Figs. 5(a)–5(c). In the empty state images, the In clusters appear as hollow-centered six-spot equilateral triangles with a distance between the spots of ~5.0 ± 0.5 Å, which is much larger than the surface lattice constant 3.84 Å of the Si(111)1×1 and the In-In nearest neighbor distance 3.25 Å. The triangular pattern is quite unusual in terms of normal close-packed structures observed previously.[26,27,36] An intuitive interpretation of the images could be that each bright spot of the triangle corresponds to an In atom, which agrees with In coverage calibration mentioned above. However, the open triangular geometry seems to be unstable in view of the loose packing, the low coordination number, and, in particular, the strong steric strain with registry to atoms on the Si substrate. Alternatively, one might attribute the six spots seen to a dynamical time averaging of more than six atoms.[20] It was recently shown that the potential energy surface of a Si adatom on Si(111)-7×7 is quite shallow.[37] Therefore, it is possible that at room temperature In atoms may hop quickly along the local energy minimum sites[20] within the basin

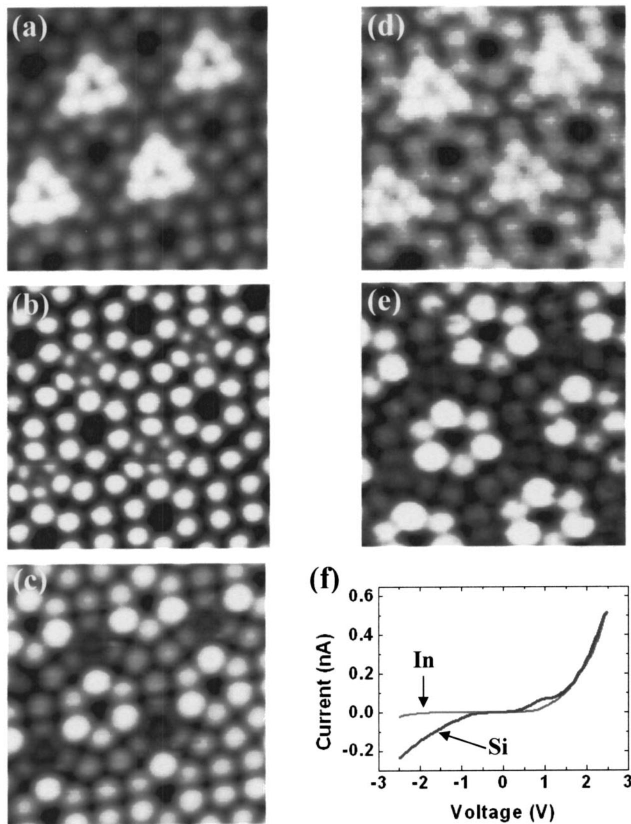

FIG. 5. Atomically resolved STM images (~5.5 nm×5.5 nm) of In clusters at bias voltage of (a) 0.6 V, (b) 0.2 V, (c) −0.3 V, respectively. (d) and (e) Low temperature (90 K) STM images at bias voltage of 0.5 and −0.3 V, respectively. (f) *I-V* curves measured on bare Si surface and on top of In clusters.

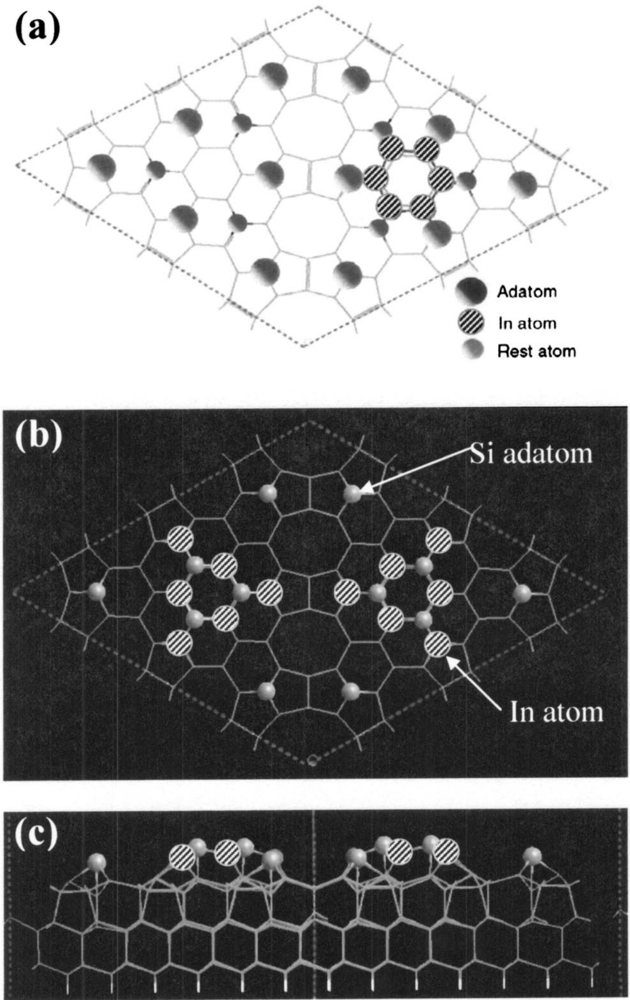

FIG. 6. (a) Top view of the honeycomb atomic structure model proposed for the In/Ga/Al six-atom cluster. (b) Top view of the atomic structure established for the In/Ga/Al cluster in this work. The big hatched balls are In/Ga/Al atoms and the small solid balls are Si adatoms. (c) Side view of the model shown in (b).

formed by one Si rest atom and three Si adatoms [Fig. 1(a)], and the six bright spots reflect these energy minimum sites with higher occupation probability. This possibility, however, can be ruled out because our STM images at ~90 K [Figs. 5(d) and 5(e)] show exactly the same patterns as in Figs. 5(a) and 5(c).

Although the appearances of the Ga and Al clusters are quite different from that of the In clusters as described above, all three kinds of clusters are imaged as triangles and consist of six bright spots in atomic resolution STM images. For both Ga and Al clusters, the distance between two edge spots is 5.5±0.5 Å, while the distance between the corner spot and neighboring edge spot is 4.6±0.5 Å. The structural model for the Ga and Al clusters cannot be obtained directly from an analysis of the STM images.

To address these puzzling issues, we carried out first-principles total energy calculations for all In, Ga, and Al clusters. A Vanderbilt ultrasoft pseudopotential[38] was used with a 100 eV cutoff energy and 1 special k point in the Brilloiun zone sum. The bare 7×7 unit cell (without counting the Si adatoms) contains six Si layers and a vacuum layer equivalent to six Si layers. We calculated the STM images following the Tersoff and Hamann formula.[39–41]

We consider three possible M (M denotes In, Ga, or Al)-cluster structures: (i) three-M-atom cluster within the triangle defined by the three Si rest atoms, $R1$ to $R3$ in Fig. 1(a), (ii) six-M-atom cluster forming a hexagonal ring [Fig. 6(a)], and (iii) six-M-atom cluster forming a hollow-centered triangle [Figs. 6(b) and 6(c)]. In case (i), each M atom is bonded to one Si rest atom, but otherwise is unable to bond to either the Si adatoms or among themselves. The coverage also disagrees with experimental coverage calibration. In case (ii), each of the six M atoms is bonded to either one of the three Si adatoms (Al-$A3$) or one of the three Si rest atoms ($R1$-$R3$). The M atoms are also bonded among themselves forming a distorted hexagonal ring. However, the simulated STM images based on this model are inconsistent with the experimental images, in particular the image for the filled states. Its energy is also 1.2 eV/cluster higher than case (iii). In case (iii), six threefold-coordinated M atoms form a triangle and three Si adatoms originally on the edge are displaced towards the triangle center considerably [Fig. 6(b)]. After optimization, it is found that the optimized structure for all three kinds of the clusters is the triangular M_6 [case (iii)] model, as demonstrated in Figs. 6(b) and 6(c).[22]

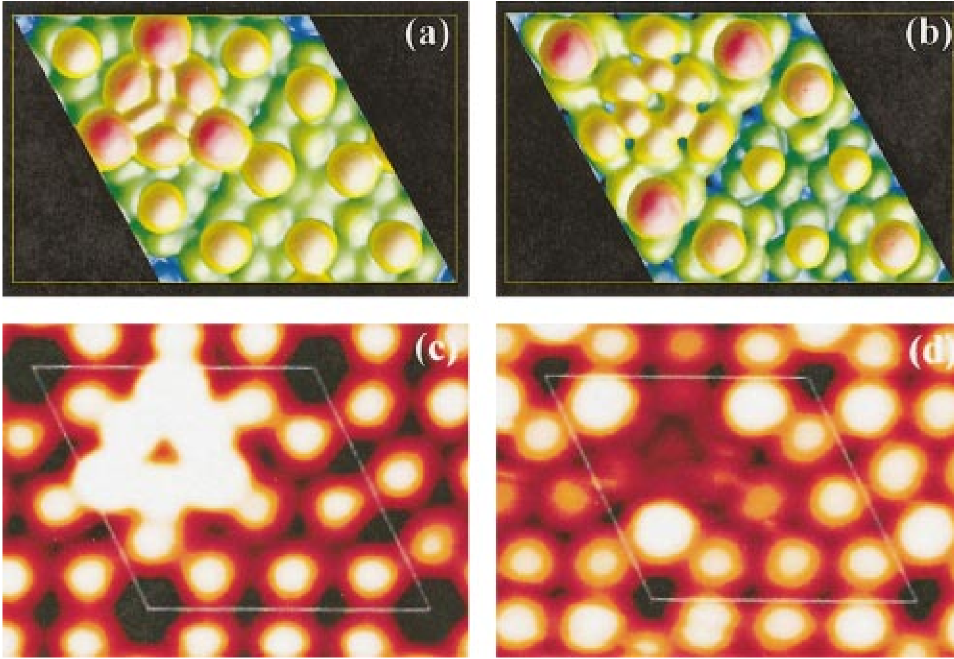

FIG. 7. (Color) The calculated STM images for the model in Figs. 6(b) and 6(c): (a) positive bias at +0.6 V and (b) negative bias at −0.3 V with respect to the Fermi energy. The color code indicates the height of the images: dark blue being low and red being high. At a typical experimental tip height of about 1 nm above the surface, only the most protruding features can be seen. For comparison, the STM images (~4.5 nm ×3.5 nm) of the In clusters recorded at sample bias voltages of +0.6 and −0.3 V are shown in (c) and (d), respectively.

The optimized parameters for the In clusters are given below. For In atoms at the corners of the triangle, the bond lengths are 2.57, 2.64, and 2.64 Å, and the bond angles are 88°, 113°, and 113°, respectively. For In atoms on the edges, the bond lengths are 2.67, 2.60, and 2.60 Å, and the bond angles are 113°, 116°, and 116°, respectively, the edge atoms are 0.30 Å higher than the three In atoms at the corners. Each of the three Si adatoms originally on the edge now bonds to three neighboring In atoms and one Si atom under it. The Si-In bond lengths are 2.598, 2.598, and 2.577 Å, and the bond angles are 124.7°, 114.6°, and 114.6°, respectively. The vertical positions of the three Si adatoms are also changed considerably. They are 0.58 Å higher than the In atoms at the corners of the triangle.

For the Ga clusters, the bond lengths of the Ga atoms at the corners of the triangle are 2.490, 2.490, and 2.430 Å, and the bond angles are 91.1°, 120.5°, and 120.5°, respectively. For the Ga atoms on the edges, the bond lengths are 2.467, 2.467, and 2.553 Å with bond angles of 115.5°, 118.9°, and 118.9°, respectively, the edge atoms are 0.30 Å higher than the three Ga atoms at the corners. Each of the three Si adatoms originally on the edge now bonds to three neighboring Ga atoms and one Si atom under it. The Si-Ga bond lengths are 2.467, 2.467, and 2.430 Å, and the bond angles are 119.7°, 114.3°, and 114.3°, respectively. The vertical positions of the three Si adatoms are also changed considerably. They are 0.69 Å higher than the Ga atoms at the corners of the triangle.

In the case of Al, the bond lengths of the Al atoms at the corners of the triangle are 2.487, 2.487, and 2.435 Å, and the bond angles are 92.6°, 122.7°, and 122.7°, respectively. For the Al atoms on the edges, the bond lengths are 2.471, 2.471, and 2.551 Å with bond angles of 115.5°, 121.0° and 121.0°, respectively, the edge atoms are 0.27 Å higher than the three Ga atoms at the corners. Each of the three Si adatoms originally on the edge now bonds to three neighboring Al atoms and one Si atom under it. The Si-Al bond lengths are 2.471, 2.471, and 2.435 Å, and the bond angles are 115.3°, 112.8°, and 112.8°, respectively. The vertical positions of the three Si adatoms are also changed considerably. They are 0.81 Å higher than the Al atoms at the corners of the triangle.

Bond angles larger than the 109.5°-tetrahedral angle are preferred as threefold group III metals prefer planar 120° bond angles (sp^2 bonding). In the $M6$ model, most bond angles of In, Ga, or Al atoms are larger than 109.5°, therefore, they are sp^2-like. Due to the considerable movements of the three Si adatoms ($A1-A3$), the three Si adatoms and the three Si rest atoms ($R1-R3$) become fourfold coordinated, removing six dangling bonds from each 7×7 unit cell. The movements of Si adatoms $A1-A3$ strengthen their bonds with the substrate atoms by resuming the 109.5°-tetrahedral angles. Similar geometries have been suggested for low energy defects in hydrogenated Si (Ref. 42) and for the *DX* center in III-V alloys.[43] Thus, displacing Si adatoms not only lets the perceived steric strain be avoided, but also lets the displaced Si adatoms serve as the "missing" links between the otherwise loosely packed M atoms.

D. Discussions

Our calculations show that an In cluster on the UFHUC is 0.1 eV/cluster higher in energy than that on the FHUC. This agrees with our experiment result very well. The calculated STM images in Figs. 7(a) and 7(b) are in remarkable qualitative agreement with experiment [Figs. 7(c) and 7(d)]. Interestingly, in the empty state image [Fig. 7(c)], the three brightest spots are from the lowest In atoms, which are 0.58 Å lower than Si $A1-A3$ with an average bond angle of 105° (thus sp^3-like). The three second-brightest spots are from the other In atoms, which are 0.28 Å lower than Si $A1-A3$ with an average bond angle of 115° (thus sp^2-like). Si adatoms $A1-A3$ are almost invisible, as they do not involve any

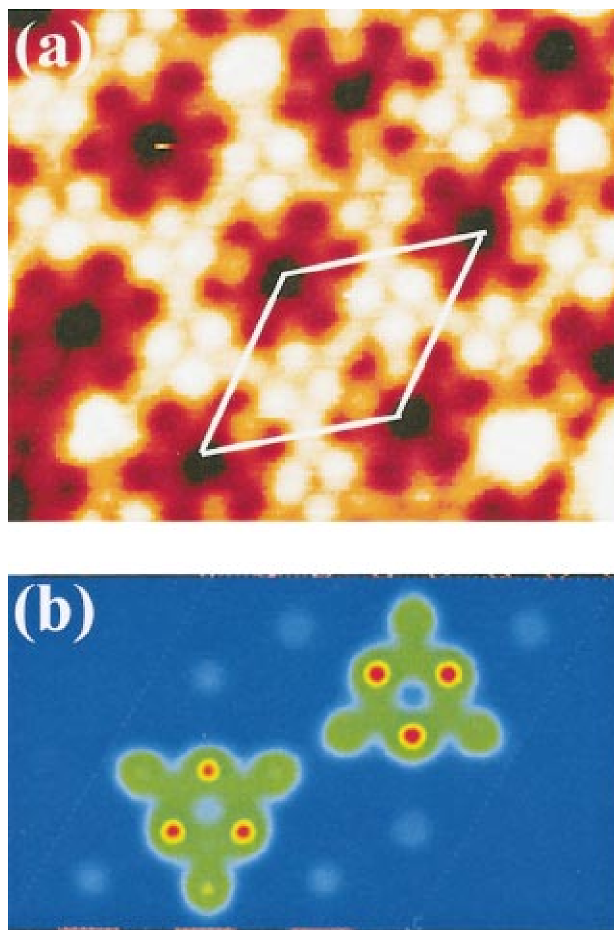

FIG. 8. (Color) (a) Atomically resolved STM image (8 nm×7 nm) of the Ga clusters recorded at +1.6 V (b) Calculated empty state STM image at a positive bias +1.6 V for the atomic model in Figs. 6(b) and 6(c). The color code indicates the image height: blue/green being low and red/yellow being high [this color notation also applies to Fig. 9(b)].

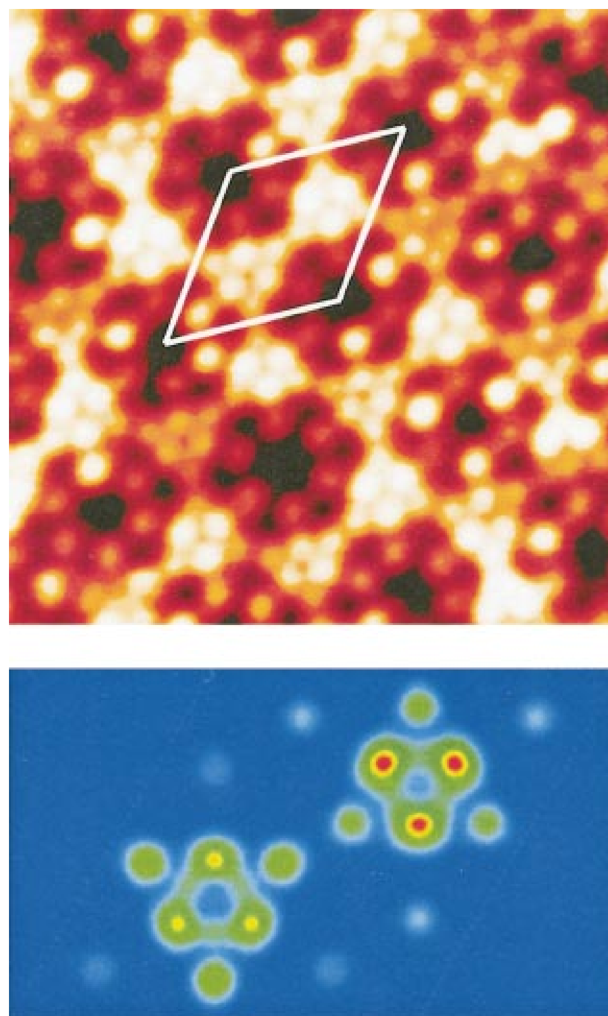

FIG. 9. (Color) (a) Atomically resolved STM image (10 nm×10 nm) of the Al clusters recorded at +1.1 V. (b) Calculated empty state STM image at a positive bias +1.1 V for the atomic model in Figs. 6(b) and 6(c).

dangling bond. A large disparity between an STM image and actual height of group III atoms has been demonstrated for an As vacancy on GaAs(110) surface.[40] Another striking feature in Fig. 7(d) is the disappearance of the six-In triangle spots under small negative bias, whereas the three Si corner adatom spots (A4–A6) become significantly brighter. Our calculation reveals that this change is not due to In diffusion but has an electronic origin. The calculated density of states reveals a 0.33 eV band gap 0.2 eV below the Fermi energy (E_F). States below the gap have mainly the Si/In bonding character. States above the gap but below E_F have mainly dangling-bond character and are predominantly on Si $A4-A6$. The In dangling bond states are found to be *above* E_F thus can only be seen in the empty state image. A micro $C-V$ profile above In clusters should reveal semiconducting characteristics. Indeed, this is confirmed by our scanning tunneling spectroscopy measurement [Fig. 5(f)] and by others.[32] Now it is possible to discuss the structure of the abnormal In clusters in Fig. 2(d). Based on the structure of the In clusters, we suggest that the abnormal In clusters in Fig. 2(d) are caused by an additional In atom adsorbed on the top of the normal In cluster. The bright spot is due to the additional In atom with an unfilled dangling bond.

Our calculations also show that the energy difference between a Ga cluster on the UFHUC and FHUC is zero within the error of the calculation. This agrees with our experimental observation very well. We have tried to grow a Ga or Al cluster triangle lattice shown in Fig. 2(b), but without success. As shown in Fig. 8, the agreement between the calculated and experimental STM images is also excellent. Unlike the In cluster, in the empty state image of the Ga cluster the most notable feature is the three brightest spots from the Ga atoms on the edge while the three Ga atoms at the corner are imaged with very weak contrast. There are two reasons for this explanation: the three Ga atoms at the corners are 0.30 Å lower than the three Ga atoms on the edge, and with an average bond angle of 110.7°, they are sp^2-like while the three In atoms at the corners are sp^3-like (see above). Similar to the In clusters, Si adatoms $A1-A3$ are almost invisible, as they do not involve any dangling bond. Interestingly, in the calculated STM image, the cluster in the FHUC is

TABLE I. M represents for Al, Ga, or In $M(\mathrm{I})$ is for the atom at corner, and $M(\mathrm{II})$ at edge, dZ is the height relative to $M(\mathrm{I})$ in Z (perpendicular to the surface) direction.

	Model	Al	Ga	In
Bond length (Å)	M(I)-Si	2.487,2.487,2.435	2.490,2.490,2.430	2.649,2.649,2.557
	M(II)-Si	2.471,2.471,2.551	2.467,2.467,2.553	2.598,2.598,2.686
	Si(A)-M	2.471,2.471,2.435	2.467,2.467,2.430	2.598,2.598,2.577
Bond angle (deg.)	M(I)-Si	92.6,122.7,122.7	91.1,120.5,120.5	87.2,113.3,113.3
	M(II)-Si	115.5,121.0,121.0	115.5,118.9,118.9	113.1,115.9,115.9
	Si(A)-M	115.3,112.8,112.8	119.7,114.3,114.3	124.7,114.6,114.6
Z position (Å)	M(I)-Si	0.0	0.0	0.0
	M(II)-Si	0.27	0.30	0.30
	Si(A)-M	0.81	0.69	0.58

slightly brighter than in the UFHUC, which is also consistent with our experiment.

As shown in Fig. 9, the contrast of the Al clusters in the FHUC is slightly sharper than in the UFHUC in the calculated STM image, which agrees well with our experiment. The STM images of the Al clusters are very similar to those of the Ga clusters. It is reasonable to use the same reasons for explaining the difference between the images of the In and Al clusters.

According to our calculations the Al clusters on the UFHUC are 0.1 eV/cluster higher in energy than those on the FHUC's. Given such energy difference, we should expect a preferential occupation of the FHUC's, as in the In case. However, in experiment the clusters equally occupy both halves of the unit cell. This is probably due to the limited Al adatom diffusion at the temperature where these clusters are formed, as evidenced by many individual Al adatoms coexisting with the clusters even at low coverage [see Fig. 4(a)]. Increasing the deposition temperature is expected to promote diffusion so that the equilibrium configuration as defined by the energy difference is reached, but this is limited by the phase transition to the Si(111)$\sqrt{3}\times\sqrt{3}$-Al and/or $\sqrt{7}\times\sqrt{7}$-Al observed in Fig. 4(d). For Al, we failed to find the experimental conditions that give rise to the triangle array with the clusters merely on the FHUC's. Thus the delicate balance between kinetics and thermodynamics for such a structure is very difficult to achieve (at least the experimental window is very narrow), which characterizes a radical difference between In and Al.

For better comparison, we list all the structure parameters of the calculated In, Ga, and Al clusters in Table I. From this table, it is easy to see that the Si-In bond lengths are larger than the Si-Al or Si-Ga bond lengths, due to the larger covalent radius of the In atom. The average bond angle of the In atoms at the corners is smaller than 109.5°, while the average bond angles of the Al and Ga atoms at the corners are larger than 109.5°. This reveals that the Al and Ga corner atoms show sp^2 bonding while the In corner atoms show sp^3 bonding, which accounts for the difference between the empty state STM images of the In clusters and Al/Ga clusters.

The results suggest that local optimization of the chemical bonds is essential for the exceptional stability of the magic clusters. The energy barrier for the In/Ga/Al atoms to reach their optimal positions is expected to be only moderate as the cluster formation involves only the insertion of In/Ga/Al into the existing 7×7 surface network that is quite flexible compared to bulk. Massive rearrangement of the surface should be avoided, as it will lead to $\sqrt{3}\times\sqrt{3}$ or other structures.[33]

In our experiments, we found that once the clusters are formed, they are fairly stable. In/Ga/Al clusters can sustain temperatures of 200, 300, and 500 °C. The higher stability of Al clusters is due to the tighter bonding between Al and Si atoms. According to our calculations, the binding energy (total energy minus atomic energy) of In_6, Ga_6, and Al_6 are −19.7, −22.3, and −25.6 eV/cell, respectively. The binding energy differences explain their different stability. It is noted that the binding energy of Al_6 is 5.9 eV/cell lower than that of In_6 on Si(111). Given such a high energy difference, it is not difficult to understand why fabrication of the ordered Al nanocluster array has been less successful.

As technologically important metal/semiconductor systems, group III metals on Si(111) have been intensively studied for more than 30 years.[32–33,35] However, no ordered array of nanoclusters has been reported before our work and a recent report on Ga.[34] There are several reasons. First, since the cluster arrays do not change the 7×7 symmetry, it is difficult to detect it without a real space high resolution technique such as STM, even if they are formed. Second, deposition of group III metals at a substrate temperature above 400 °C or post annealing of room temperature prepared samples usually results in $\sqrt{3}\times\sqrt{3}$ or other reconstructions.[33] In this case, nanoclusters do not form. The growth conditions are very important for such nanocluster formation, and the window is very narrow, which is probably the most important reason why these nanoclusters were not found in previous studies. In our experiments, we found that the optimized conditions are ~0.05 ML/min (the deposition rate) and 100–200 °C (the substrate temperature) for In, ~0.02 ML/min and ~150–250 °C for Ga, and 0.01 ML/min and 250–350 °C for Al, respectively. Once these parameters are established, the ordered array can be routinely fabricated. We can see that from In to Al, lower deposition rates and higher substrate temperatures are needed for uniform clusters formation. This can be understood in terms of the big difference in the dif-

fusivities of In, Ga, and Al. Due to the stronger interaction between Al and Si, the Al adatoms cannot diffuse fast enough to reach the right positions for forming clusters at lower substrate temperature.

IV. CONCLUSIONS

The technique of "template plus magic clustering" has been successfully used to fabricate ordered arrays of In/Ga/Al nanoclusters with identical size. There is essentially no limitation to this strategy as long as the atoms of a specific material to be grown can form clusters of definite size, and the substrate template used to accumulate and separate these entities can be properly selected. This is demonstrated by fabricating more than ten different nanocluster arrays with other metals and alloys, including Mn, Ag, K,[44] In/Mn, and Ag/In.[22] The high stability, perfect ordering, and identical size of the In/Ga/Al nanoclusters are important factors for practical applications, and these artificial nanocluster crystals may open a field to study the properties of nanostructures and to explore new functionalities. A recent example is the observation of ferromagnetism in one-dimensional metal monoatomic chains,[45] and we expect that some similar effects might exist in the Mn nanocluster array.[44]

ACKNOWLEDGMENTS

The work at IOP was supported by a grant from China NSF (Grant Nos. 69625608, 10174089). Work at NREL was supported by U.S. DOE/OS/BES under Contract No. DE-AC36-99GO10337, and by DOE/NERSC for supercomputer time, and by Oak Ridge National Laboratory, managed by UT-Battell, LLC for the U.S. DOE under Contract No. DE-AC05-00OR22725, and by the U.S. NSF (Grant No. DMR-0071893), respectively.

[1] M. Valden, X. Lai, and D. W. Goodman, Science **281**, 1647 (1998).
[2] M. Haruta, Catal. Today **36**, 153 (1997).
[3] A. O. Orlov, I. Amlani, G. H. Bernstein, C. S. Lent, and G. L. Snider, Science **277**, 928 (1997).
[4] R. P. Andres, T. Bein, M. Dorogi, S. Feng, J. I. Henderson, C. P. Kubiak, W. Mahoney, R. G. Osifchin, and R. Reifenberger, Science **272**, 1323 (1996).
[5] T. W. Kim, D. C. Choo, J. H. Shim, and S. O. Kang, Appl. Phys. Lett. **80**, 2168 (2002).
[6] S. Sun, C. B. Murray, D. Weller, L. Folks, and A. Moser, Science **287**, 1989 (2000).
[7] K. Koike, H. Matsuyama, Y. Hirayama, K. Tanahashi, T. Kanemura, O. Kitakami, and Y. Shimada, Appl. Phys. Lett. **78**, 874 (2001).
[8] T. Koide, H. Miyauchi, J. Okamoto, T. Shidara, A. Fujimori, H. Fukutani, K. Amemiya, H. Rakeshita, S. Yuasa, T. Katayama, and Y. Suzuki, Phys. Rev. Lett. **87**, 257201 (2001).
[9] P. M. Petroff, A. Lorke, and A. Imamoglu, Phys. Today **May**, 46 (2001).
[10] V. F. Puntes, K. M. Krishnan, and A. P. Alivisatos, Science **291**, 2115 (2001).
[11] C. T. Black, C. B. Murray, R. L. Sandstrom, and S. H. Sun, Science **290**, 1131 (2000).
[12] P. L. McEuen, Science **278**, 1729 (1997).
[13] K. Bromann, C. Félix, H. Brune, W. Harbich, R. Monot, J. Buttet, and K. Kern, Science **274**, 956 (1996).
[14] H. Brune, M. Glovannini, K. Bromann, and K. Kern, Nature (London) **394**, 451 (1998).
[15] M. Hwang, M. C. Abraham, T. A. Savas, H. I. Smith, R. J. Ram, and C. A. Ross, J. Appl. Phys. **87**, 5108 (2000).
[16] R. O'Barr, S. Y. Yamamoto, S. Schults, W. Xu, and A. Scherer, J. Appl. Phys. **81**, 4730 (1997).
[17] D. M. Eigler and E. K. Schweizer, Nature (London) **344**, 524 (1990).
[18] A. D. Kent, S. Molnar, S. Gider, and D. D. Awschalom, J. Appl. Phys. **76**, 6656 (1994).
[19] M. Yoon, X. F. Lin, I. Chizhov, H. Mai, and R. F. Willis, Phys. Rev. B **64**, 085321 (2001).
[20] L. Vitali, M. G. Ramsey, and F. P. Netzer, Phys. Rev. Lett. **83**, 316 (1999).
[21] Y. P. Zhang, L. Yan, S. S. Xie, S. J. Pang, and H. J. Gao, Surf. Sci. **497**, L60 (2002).
[22] J. L. Li, J. F. Jia, X. J. Liang, X. Liu, J. Z. Wang, Q. K. Xue, Z. Q. Li, J. S. Tse, Z. Y. Zhang, and S. B. Zhang, Phys. Rev. Lett. **88**, 066101 (2002).
[23] J. F. Jia, J. Z. Wang, X. Liu, Q. K. Xue, Z. Q. Li, Y. Kawazoe, and S. B. Zhang, Appl. Phys. Lett. **80**, 3186 (2002).
[24] J. L. Li, X. J. Liang, J. F. Jia, X. Liu, J. Z. Wang, E. G. Wang, and Q. K. Xue, Appl. Phys. Lett. **79**, 2826 (2001).
[25] W. D. Knight, K. Clemenger, W. A. de Heer, W. A. Saunders, M. Y. Chou, and M. L. Cohen, Phys. Rev. Lett. **52**, 2141 (1984).
[26] D. M. Chen, J. A. Golovchenco, P. Bedrossian, and K. Mortensen, Phys. Rev. Lett. **61**, 2867 (1988).
[27] M. Y. Lai and Y. L. Wang, Phys. Rev. Lett. **81**, 164 (1998).
[28] F. Liu, M. Mostoller, T. Kaplan, S. N. Khanna, P. Jena, Chem. Phys. Lett. **248**, 213 (1996).
[29] K.-J. Jin, G. D. Mahan, H. Metiu, and Z. Y. Zhang, Phys. Rev. Lett. **80**, 1026 (1998).
[30] K. Takayanagi, Y. Tanishiro, M. Takahashi, and S. Takahashi, J. Vac. Sci. Technol. A **3**, 1502 (1985); G.-X. Qian and D. J. Chadi, Phys. Rev. B **35**, 1288 (1987).
[31] Z. Zhang and Max. G. Lagally, Science **276**, 377 (1997).
[32] X. F. Lin, H. A. Mai, I. Chizhov, and R. F. Willis, J. Vac. Sci. Technol. B **14**, 995 (1996).
[33] J. Kraft, M. G. Ramsey, and F. P. Netzer, Phys. Rev. B **55**, 5384 (1997).
[34] M. Y. Lai and Y. L. Wang, Phys. Rev. B **64**, 241404 (2001).
[35] R. J. Hamers, Phys. Rev. B **40**, 1657 (1989).
[36] I.-S. Hwang, M.-S. Ho, and T. T. Tsong, Phys. Rev. Lett. **83**, 120 (1999).
[37] K. Cho and E. Kaxiras, Surf. Sci. **396**, L261 (1998).
[38] D. Vanderbilt, Phys. Rev. B **41**, 7892 (1990).
[39] J. Tersoff and D. R. Hamann, Phys. Rev. B **31**, 805 (1985).

[40] S. B. Zhang and A. Zunger, Phys. Rev. Lett. **77**, 119 (1996).
[41] T. Hitotsugi, S. Heike, T. Onogi, T. Hashizume, S. Watanabe, Z.-Q. Li, K. Ohno, Y. Kawazoe, T. Hasegawa, and K. Kitazawa, Phys. Rev. Lett. **82**, 4034 (1999).
[42] R. Biswas and Y.-P. Li, Phys. Rev. Lett. **82**, 2512 (1999).
[43] S. B. Zhang and D. J. Chadi, Phys. Rev. B **42**, 7174 (1990).
[44] J. Z. Wang, J. F. Jia, X. J. Liang, X. Liu, and Q. K. Xue (unpublished).
[45] P. Gambardella, A. Dallmeyer, K. Maiti, M. C. Malagoli, W. Eberhardt, K. Kern, and C. Carbone, Nature (London) **416**, 301 (2002).